论著·临床医学

# CT-临床列线图预测甲状腺微小乳头状癌中央区淋巴结转移

范 锐[1],贺星云[1],杜俊泽[2],陈林丽[3] 陆军军医大学(第三军医大学)第一附属医院:[1]放射科,[2]乳腺甲状腺外科,重庆;[3]重庆医科大学附属第二医院放射科,重庆

[摘要] **目的** 探讨基于CT影像特征联合临床因素构建列线图模型对甲状腺微小乳头状癌(papillary thyroid microcarcinoma,PTMC)患者中央区淋巴结转移(central lymph node metastasis,CLNM)的预测价值。**方法** 采用病例-对照研究方法,纳入2022年1月至2024年11月2家三甲医院256例经病理证实的PTMC患者,所有患者术前2周内接受颈部增强CT扫描,并行中央区淋巴结清扫术。陆军军医大学第一附属医院201例,以7∶3的比例简单随机抽样分为训练集($n$=140)和内部测试集($n$=61);重庆医科大学附属第二医院的55例患者作为外部测试集。收集患者临床资料及CT影像特征,通过单因素及多因素Logistic回归分析筛选CLNM独立预测因子,构建列线图模型。采用受试者工作特征曲线(receiver operating characteristic,ROC)、曲线下面积(area under the curve,AUC)、校准曲线及决策曲线分析(decision curve analysis,DCA)评估模型区分度、校准度及临床有效性。**结果** 多因素Logistic分析显示,男性($OR$=5.991,95%$CI$:2.209~18.350)、肿瘤最大直径≥0.82 cm($OR$=18.880,95%$CI$:1.803~229.500)、被膜累及($OR$=9.805,95%$CI$:4.015~26.340)、CT诊断淋巴结($OR$=2.872,95%$CI$:1.176~7.232)为CLNM独立预测因子($P$<0.05)。列线图模型在训练集、内部测试集和外部测试集的AUC分别为0.859(95%$CI$:0.796~0.922)、0.786(95%$CI$:0.671~0.901)和0.783(95%$CI$:0.648~0.917),校准曲线显示预测概率与实际概率高度一致(Hosmer-Lemeshow检验$P$>0.05)。决策曲线分析表明,当阈值概率为0.18~0.80时,模型可显著提高CLNM术前识别净获益率。**结论** 基于性别、肿瘤最大直径、被膜累及和CT诊断淋巴结构建的列线图模型能有效预测PTMC患者CLNM风险,为个体化手术方案制定提供量化工具,具有较高临床应用价值。

[关键词] 甲状腺微小乳头状癌;中央区淋巴结转移;X线计算机体层摄影术;预测模型
[中图法分类号] R730.44;R730.7;R736.1 [文献标志码] A

# Predictive nomogram for central lymph node metastasis in papillary thyroid microcarcinoma based on CT-clinical data

FAN Rui[1], HE Xingyun[1], DU Junze[2], CHEN Linli[3] [1]Department of Radiology, [2]Department of Breast and Thyroid Surgery, First Affiliated Hospital, Army Medical University (Third Military Medical University), Chongqing; [3]Department of Radiology, the Second Affiliated Hospital of Chongqing Medical University, Chongqing, China

[**Abstract**] **Objective** To investigate the predictive value of a nomogram for central lymph node metastasis (CLNM) in patients with papillary thyroid microcarcinoma (PTMC) based on CT features combined with clinical factors. **Methods** A case-control study was conducted on 256 pathologically confirmed PTMC

[基金项目] 重庆市技术创新与应用发展专项重点项目(CSTC2021jscx-gksb-N0025)
[通信作者] 陈林丽,E-mail:282343684@qq.com

2097-0927/Copyright © 2025,陆军军医大学(第三军医大学)。这篇开放获取文章遵循CC BY许可协议(https://creativecommons.org/licenses/by/4.0/)
**引用格式**:范锐,贺星云,杜俊泽,等.CT-临床列线图预测甲状腺微小乳头状癌中央区淋巴结转移[J].陆军军医大学学报,2025,47(18):2245-2253. DOI:10.16016/j.2097-0927.202506025.
**Citation**:FAN RUI,HE XINGYUN,DU JUNZE, *et al*. Predictive nomogram for central lymph node metastasis in papillary thyroid microcarcinoma based on CT-clinical data[J]. J Army Med Univ,2025,47(18):2245-2253. DOI:10.16016/j.2097-0927.202506025.

patients from 2 tertiary hospitals from January 2022 to November 2024. All participants underwent contrast-enhanced neck CT scanning within 2 weeks before surgery and received central lymph node dissection. The 201 patients from the First Affiliated Hospital of Army Medical University were randomized into a training set ($n$=140) and an internal validation set ($n$=61) in a 7∶3 ratio. The 55 patients from the Second Affiliated Hospital of Chongqing Medical University were all assigned into an external validation set. Their clinical data and CT features were collected. Univariate and multivariate logistic regression analyses were employed to identify independent predictive factors for CLNM, and then a nomogram model was constructed. Receiver operating characteristic (ROC) curve analysis (area under the curve, AUC), calibration curve, and decision curve analysis (DCA) were performed to evaluate the model performance, discrimination and clinical utility. **Results** Multivariate logistic regression analysis identified 4 independent CLNM predictors ($P$<0.05), that is, male ($OR$=5.991, 95%$CI$: 2.209~18.350), tumor size ≥0.82 cm ($OR$=18.880, 95%$CI$: 1.803~229.500), capsular involvement ($OR$=9.805, 95%$CI$: 4.015~26.340), and CT-diagnosed lymph node positivity ($OR$=2.872; 95%$CI$: 1.176~7.232). The nomogram achieved an AUC value of 0.859 (95%$CI$: 0.796~0.922), 0.786 (95%$CI$: 0.671~0.901), and 0.783 (95%$CI$: 0.648~0.917) in the training and internal and external validation sets, respectively. Calibration curves demonstrated high consistency between predicted and observed probabilities (Hosmer-Lemeshow $P$>0.05). DCA confirmed net clinical benefits for CLNM before surgical treatment with a threshold probability range of 0.18~0.80. **Conclusion** Based on sex, tumor size, capsular involvement, and CT-diagnosed lymph node metastasis, our nomogram model effectively predicts CLNM risk in PTMC patients. It can be used as a quantitative tool for personalized surgical planning and shows high clinical applicability.

[**Key words**] papillary thyroid microcarcinoma; central lymph node metastasis; X-ray computed tomography; prediction model

Supported by the Key Special Project of Technological Innovation and Application Development of Chongqing (CSTC2021jscx-gksb-N0025). Corresponding author: CHEN Linli, E-mail: 282343684@qq.com

甲状腺癌的发病率在全球范围内显著增加,尤其是甲状腺乳头状癌(papillary thyroid carcinoma,PTC)的病例数在过去三十年中大幅上升[1]。在这些病例中,甲状腺微小乳头状癌(papillary thyroid microcarcinoma,PTMC)占据了相当大的比例,约为新发甲状腺癌病例的三分之一[2]。随着影像技术的进步,尤其是高分辨率超声的广泛应用,许多小型甲状腺癌得以被偶然发现,这也导致了PTMC的诊断率上升[3]。尽管PTMC进展缓慢,预后相对较好,但淋巴结转移经常发生在早期,尤其是中央区淋巴结转移(central lymph node metastasis, CLNM),这一现象会增加远处转移和复发的风险[4]。在PTMC患者中,过度的外科手术可能会导致一系列并发症。研究表明,尽管手术是治疗PTMC的一种常见方法,但并不是所有患者都需要立即进行手术干预,事实上,早期的外科手术可能会增加并发症的风险,而不是预防这些并发症[5]。因此,对CLNM进行全面的术前评估对于优化手术策略和改善患者结局至关重要。

美国甲状腺协会(American Thyroid Association,ATA)指南强调了术前评估原发肿瘤和颈部淋巴结以指导手术决策的重要性[6]。术前颈部超声(ultrasound,US)和US引导下的细针穿刺(fine needle aspiration,FNA)活检是检测PTMC患者淋巴结转移的主要诊断工具[7]。然而,颈部US的诊断性能因从业者而异,在评估CLNM时,观察者间的可变性最高[8-9]。一项涉及31 942名患者的42项研究的荟萃分析报告显示,US预测CLNM的综合敏感性较低,为28%[10]。CT成像可以显著减少CLNM的漏诊,改善手术计划[11]。尽管CT扫描具有优势,但其在PTMC患者术前评估中的全部潜力往往未得到充分利用,因为CT提供了对原发肿瘤及其与周围组织(包括淋巴结转移)的关系的重要见解,这对于确定淋巴结清扫的程度至关重要。因此,本研究旨在完善PTMC患者中央区淋巴结清扫的决策过程,开发一种CT-临床模型预测PTMC患者的CLNM,为精确的手术治疗计划提供循证支持。

## 1 资料与方法

### 1.1 研究对象

本研究采用病例-对照研究方法,经陆军军医大学第一附属医院伦理委员会批准[(B)KY2023099],并且免除了知情同意的需要。回顾性收集了2022年1月至2024年11月期间2个中心256例经组织病理学验证的PTMC患者的数据,包括年龄、性别、身体质量指数(body mass index,BMI)、病程、肿瘤最大直径、T3、T4、FT3、FT4、是否有结节性甲状腺肿、是否有甲状腺炎、促甲状腺激素(thyroid stimulating hormone,TSH)、抗甲状腺过氧化物酶抗体(thyroid peroxidase antibody,TPoab)、抗甲状腺球蛋白抗体(thyroglobulin antibody,TGAb)、甲状腺球蛋白(thyroglobulin,TG)。中心1(陆军军医大学第一附属医院乳腺甲状腺外科)201例,采用简单随机抽样将患者以7∶3的比例随机分为训练集($n$=140例)和内部测试集($n$=61例)。将中心2(重庆医科大学附属第二医院放射科)55例患者作为外部测试集。纳入标准:①术前2周进行颈部CT增强扫描;②术后病理确诊为PTC;③患者已行颈部淋巴结清扫术,且切除淋巴结均有病理诊断;④临床病理资料完整。排除标准:①患者临床病理资料不完整;②CT图像不全。

### 1.2 样本量计算

本研究根据每个变量事件(events per variable,EPV)指标计算样本量,根据前期调研[12]和预试验计算样本量,预期CLNM发生率约为30%,进入回归分析的因素有4个(性别、肿瘤最大直径、被膜累及、CT诊断淋巴结),依据样本量计算公式:样本量=变量数×10÷事件发生率,本研究所需样本量不少于134例(4×10÷0.3≈133.33例)。

### 1.3 仪器与检查方法

采用德国Siemens公司的Somatom Definition AS 64排螺旋CT机或Somatom Definition Flash双源螺旋CT机扫描。扫描参数:管电压140 kV,管电流为自动设置,螺距为1.2~1.5。增强扫描采用非离子型对比剂碘海醇(含碘300 mg/mL),注射剂量80~100 mL,注射速度3.5~4.0 mL/s,于升主动脉内取约1 $cm^2$大小的圆形感兴趣区(region of interest,ROI),对比剂开始注射10 s后进行连续轴向扫描,在实时重建图像上当其CT值达到触发阈值(120 HU)后进行动脉期扫描,顺延15~20 s进行静脉期扫描。重建参数:软组织窗位30~60 HU,窗宽200~450 HU,层间距1 mm,层厚1 mm。

### 1.4 图像分析

由2名工作经验丰富的影像科医师(分别工作10年和11年)以双盲法对CT图像形态学特征进行评估,有异议时讨论后决定。两名医师观察CT薄层图像并记录以下特征:①位置分为甲状腺上叶、甲状腺中叶、甲状腺下叶、甲状腺峡部;②结节形态是否规则;③有无被膜累及;④有无钙化。颈部淋巴结出现以下5项CT影像征象中的1项时,CT诊断为转移性淋巴结:①明显增强(CT值>40 HU);②最小直径/最大直径>0.5;③淋巴结囊变,淋巴结微钙化,淋巴结簇状聚集(同组淋巴结≥3枚);④颈部淋巴结的最小径>10 mm;⑤淋巴结门的消失。

### 1.5 统计学分析

采用R Studio软件(4.4.2版,www.r-project.org)用于统计分析。符合正态分布的计量资料采用$\bar{x}\pm s$表示,组间比较采用$t$检验;不符合正态分布的连续性变量采用$M(P_{25},P_{75})$表示,组间比较采用Mann Whitney $U$检验。计数资料以例(%)表示,采用$\chi^2$检验。采用多因素二元Logistic回归分析PTMC中央区淋巴结转移的相关因素,绘制受试者工作特征曲线(receiver operating characteristic curve,ROC)评估列线图模型预测PTMC中央区淋巴结转移的价值。绘制校准曲线以评估综合模型的拟合优度,决策曲线评估综合模型的临床效用。$P$<0.05表示差异具有统计学意义。

## 2 结果

### 2.1 术前临床资料及影像资料比较.

训练集包括140名患者(平均年龄43.6±11.5岁,97名女性),内部测试集包括61名患者(平均年龄43.2±10.1岁,41名女性),外部测试集包括55名患者(平均年龄41.2±11.1岁,41名女性)。在所有队列中125例(49%)发生转移(表1)。训练集组间比较结果显示:性别、肿瘤最大直径、被膜累及、CT诊断淋巴结组间比较差异有统计学意义($P$<0.05,表2),2组其他临床及影像资料比较,差异均无统计学意义。2组典型病例见图1。

### 2.2 列线图模型的建立

根据多因素分析中各因素β值构建PTMC中央区淋巴结转移的预测模型为:P=eX/(1+eX);其中e为自然对数,X=-4.435+1.79×性别+2.938×肿瘤最大直径+2.283×被膜累及+1.055×CT诊断淋巴结。通过绘制列线图实现模型的可视化(图2)。

表1 PTMC患者在训练集、测试集及外部测试集中的临床信息特征[$\bar{x}\pm s$, 例(%),$M(P_{25},P_{75})$]

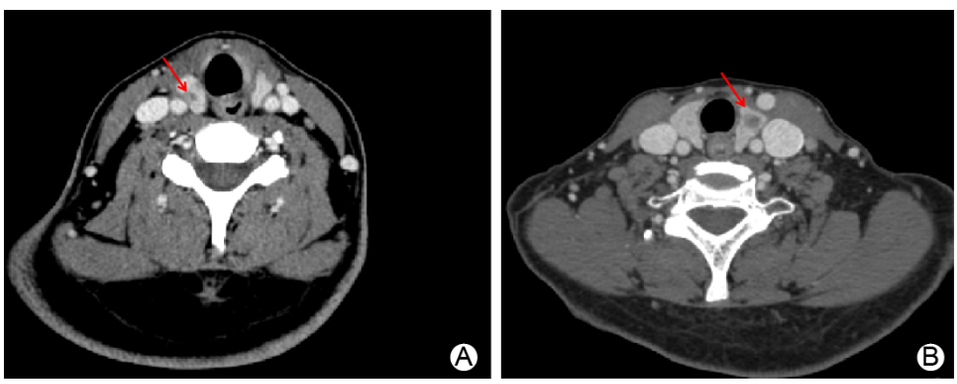
Table 1 PTMC involvement of the capsule as shown on enhanced CT images [$\bar{x}\pm s$, $n$(%),$M(P_{25},P_{75})$]

| Variables | Training Set($n$=140) | | $P$ | Internal Test Set($n$= 61) | | $P$ | External Test Set($n$= 55) | | $P$ |
|---|---|---|---|---|---|---|---|---|---|
| | No Metastasis ($n$=63) | Metastasis ($n$=77) | | No Metastasis ($n$=29) | Metastasis ($n$=32) | | No Metastasis ($n$=39) | Metastasis ($n$=16) | |
| Sex | | | 0.004 | | | 0.273 | | | 0.519 |
| Female | 52 (83) | 45 (58) | | 22 (76) | 19 (59) | | 30 (77) | 11 (69) | |
| Male | 11 (17) | 32 (42) | | 7 (24) | 13 (41) | | 9 (23) | 5 (31) | |
| Age/years | 43.95±12.29 | 43.32±10.79 | 0.751 | 46.90±9.01 | 40.00±10.03 | 0.006 | 46.31±11.25 | 38.56±11.42 | 0.030 |
| Nodular goiter | | | 0.437 | | | 1.000 | | | 0.200 |
| No | 48 (76) | 53 (69) | | 24 (83) | 27 (84) | | 38 (97) | 14 (88) | |
| Yes | 15 (24) | 24 (31) | | 5 (17) | 5 (16) | | 1 (3) | 2 (12) | |
| Thyroiditis | | | 1.000 | | | 0.140 | | | 1.000 |
| No | 45 (71) | 54 (70) | | 24 (83) | 20 (62) | | 28 (72) | 12 (75) | |
| Yes | 18 (29) | 23 (30) | | 5 (17) | 12 (38) | | 11 (28) | 4 (25) | |
| Tumor maximum diameter/cm | 0.73±0.19 | 0.84±0.15 | <0.001 | 0.79 (0.61, 0.88) | 0.83 (0.70, 0.93) | 0.203 | 0.63±0.16 | 0.66±0.18 | 0.480 |
| Course/months | 2 (1.00, 5.50) | 2 (1.00, 12.00) | 0.931 | 1 (0.70, 12.00) | 1 (1.00, 4.25) | 0.901 | 1(0.33, 24.00) | 0.23 (0.22, 1.25) | 0.057 |
| T3/(nmol/L) | 1.91 (1.69, 2.10) | 1.94 (1.72, 2.20) | 0.642 | 1.92 (1.72, 2.28) | 1.81 (1.62, 2.05) | 0.177 | 1.80 (1.57, 2.02) | 1.90 (1.67, 2.30) | 0.340 |
| T4/(nmol/L) | 106.10 (94.48, 118.75) | 104.80 (90.24, 113.90) | 0.491 | 107.80 (102.1, 125.2) | 104.06 (95.32, 118.58) | 0.143 | 106.00 (96.74, 114.70) | 111.50 (104.12,124.33) | 0.331 |
| FT3/(pmol/L) | 4.93 (4.50, 5.46) | 4.95 (4.49, 5.47) | 0.877 | 5.13 (4.45, 5.51) | 5.04 (4.58, 5.43) | 0.994 | 4.64 (4.20, 5.08) | 4.47 (3.88, 5.25) | 0.810 |
| FT4/(pmol/L) | 16.89 (15.25, 18.91) | 16.86 (14.70, 18.74) | 0.549 | 18.09±3.04 | 16.91±2.68 | 0.115 | 16.50 (14.86, 18.06) | 16.05 (14.47, 17.7) | 0.732 |
| TSH/(μIU/mL) | 1.92 (1.27, 2.56) | 2.16 (1.44, 3.09) | 0.201 | 1.92 (1.31, 2.66) | 1.90 (1.43, 2.62) | 0.828 | 1.93 (1.30, 2.87) | 2.05 (0.92, 2.77) | 0.760 |
| TG/(ng/mL) | 9.82 (1.94, 18.7) | 9.96 (3.72, 21.87) | 0.559 | 11.30 (1.29, 13.76) | 12.38 (2.28, 25.08) | 0.196 | 6.99 (1.60, 12.18) | 8.47 (2.65, 13.97) | 0.643 |
| TGAb/(IU/mL) | 19.56 (11.18, 44.7) | 18.70 (10.07, 60.83) | 0.766 | 22.03 (6.99, 99.83) | 26.93 (18.06, 120.18) | 0.228 | 23.20 (19.32, 153.84) | 31.59 (22.77, 54.50) | 0.335 |
| TMAb/% | 4.87 (3.45, 9.85) | 6.21 (3.64, 12.48) | 0.346 | 5.77 (3.85, 19.39) | 6.81 (3.50, 18.43) | 1.000 | 8.89 (3.29, 21.81) | 4.81 (3.73, 9.88) | 0.517 |
| TPoab/(IU/mL) | 21.17 (9.14, 35.52) | 18.98 (9.37, 36.02) | 0.940 | 22.34 (12.49, 36.42) | 21.00 (13.98, 38.20) | 0.862 | 23.07 (12.85, 46.99) | 19.66 (10.55, 31.99) | 0.415 |
| BMI/(kg/m$^2$) | 24.08±4.62 | 24.8±3.44 | 0.307 | 24.57±4.34 | 24.2±3.87 | 0.731 | 23.78±3.72 | 23.94±3.65 | 0.879 |
| Location | | | 0.640 | | | 0.364 | | | 0.966 |
| Isthmus | 4 (6) | 7 (9) | | 1 (3) | 3 (9) | | 2 (5) | 1 (6) | |
| Up | 21 (33) | 32 (42) | | 13 (45) | 8 (25) | | 14 (36) | 5 (31) | |
| Middle | 22 (35) | 23 (30) | | 8 (28) | 13 (41) | | 15 (38) | 7 (44) | |
| Lower | 16 (25) | 15 (19) | | 7 (24) | 8 (25) | | 8 (21) | 3 (19) | |
| Calcification | | | 1.000 | | | 0.796 | | | 0.165 |
| No | 45 (71) | 56 (73) | | 19 (66) | 23 (72) | | 33 (85) | 16 (100) | |
| Yes | 18 (29) | 21 (27) | | 10 (34) | 9 (28) | | 6 (15) | 0 | |
| Irregular shape | | | 0.785 | | | 0.240 | | | 0.892 |
| No | 31 (49) | 35 (45) | | 18 (62) | 14 (44) | | 22 (56) | 8 (50) | |
| Yes | 32 (51) | 42 (55) | | 11 (38) | 18 (56) | | 17 (44) | 8 (50) | |

续表1 PTMC患者在训练集、测试集及外部测试集中的临床信息特征[$\bar{x}\pm s$, 例(%),$M(P_{25},P_{75})$]

Table 1(continued) PTMC involvement of the capsule as shown on enhanced CT images [$\bar{x}\pm s$, $n$(%),$M(P_{25},P_{75})$]

| Variables | Training Set($n$=140) | | $P$ | Internal Test Set($n$=61) | | $P$ | External Test Set($n$=55) | | $P$ |
|---|---|---|---|---|---|---|---|---|---|
| | No Metastasis ($n$=63) | Metastasis ($n$=77) | | No Metastasis ($n$=29) | Metastasis ($n$=32) | | No Metastasis ($n$=39) | Metastasis ($n$=16) | |
| Membrane involvement | | | <0.001 | | | <0.001 | | | <0.001 |
| No | 42 (67) | 13 (17) | | 20 (69) | 6 (19) | | 30 (77) | 4 (25) | |
| Yes | 21 (33) | 64 (83) | | 9 (31) | 26 (81) | | 9 (23) | 12 (75) | |
| CT diagnosis of lymph nodes | | | <0.001 | | | 0.161 | | | <0.001 |
| No | 47 (75) | 33 (43) | | 23 (79) | 19 (59) | | 28 (72) | 3 (19) | |
| Yes | 16 (25) | 44 (57) | | 6 (21) | 13 (41) | | 11 (28) | 13 (81) | |




A: A 40-year-old female patient. The red arrow indicates that the enhanced CT scan shows an incomplete tumor capsule, and the degree of enhancement is lower than that of the surrounding normal thyroid tissue, presenting an interrupted margin, suggesting involvement of the thyroid capsule. B: A 55-year-old female patient. The enhanced scan shows a complete tumor capsule (red arrow), and the degree of enhancement is lower than that of the surrounding normal thyroid tissue, without involvement of the thyroid capsule

图1 PTMC被膜累及情况增强CT影像

Figure 1 PTMC involvement of the capsule as shown on enhanced CT images

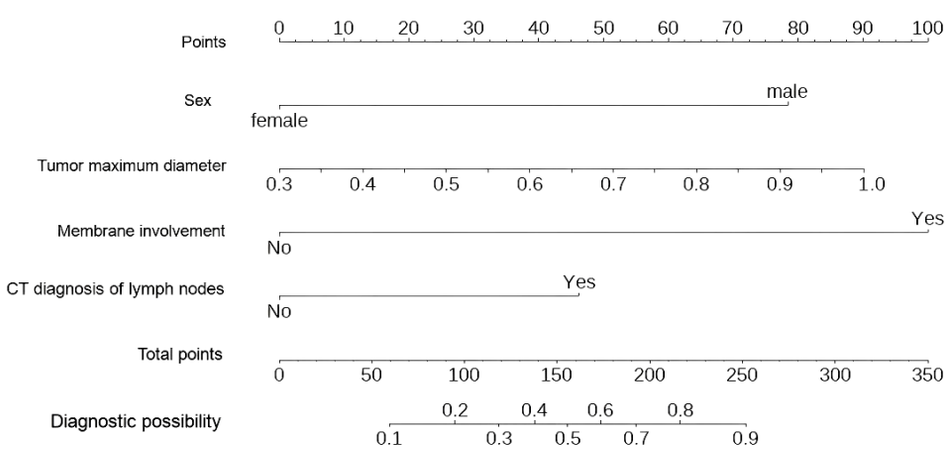



图2 甲状腺微小乳头状癌中央区淋巴结转移发生风险列线图预测模型

Figure 2 Nomogram prediction model for the risk of central lymph node metastasis in papillary thyroid microcarcinoma

表2 预测PTMC中央区淋巴结转移临床特征单因素和多因素Logistic回归结果

Table 2 Univariate Cox regression analysis of OS in *NPM1*m-AML patients

| Variables | Univariate Analysis | | | Multivariate Analysis | | |
|---|---|---|---|---|---|---|
| | *OR*(95%*CI*) | *Z* | *P* | *OR*(95%*CI*) | *Z* | *P* |
| Age/years | 0.995(0.966~1.025) | −0.324 | 0.746 | | | |
| Sex | 3.362(1.558~7.692) | 2.997 | 0.003 | 5.991(2.209~18.350) | 3.344 | <0.001 |
| BMI/(kg/m$^2$) | 1.047(0.962~1.144) | 1.048 | 0.295 | | | |
| CT diagnosis of lymph nodes | 3.917(1.927~8.258) | 3.691 | <0.001 | 2.872(1.176~7.232) | 2.293 | <0.050 |
| Membrane involvement | 9.846(4.568~22.490) | 5.648 | <0.001 | 9.805(4.015~26.340) | 4.800 | <0.001 |
| Irregular shape | 1.162(0.596~2.271) | 0.442 | 0.658 | | | |
| Calcification | 0.938(0.446~1.981) | −0.171 | 0.865 | | | |
| Course/months | 0.996(0.973~1.019) | −0.349 | 0.727 | | | |
| Tumor maximum diameter/cm | 35.450(4.791~304.000) | 3.387 | 0.001 | 18.880(1.803~229.500) | 2.395 | <0.050 |
| Thyroiditis | 1.065(0.513~2.234) | 0.168 | 0.867 | | | |
| Nodular goiter | 1.449(0.687~3.128) | 0.964 | 0.335 | | | |
| Location | | | | | | |
| Isthmus | | | | | | |
| Up | 0.871(0.207~3.259) | −0.202 | 0.840 | | | |
| Middle | 0.597(0.140~2.265) | −0.742 | 0.458 | | | |
| Lower | 0.536(0.120~2.150) | −0.864 | 0.388 | | | |
| TPoab/(IU/mL) | 1.000(0.996~1.005) | 0.221 | 0.825 | | | |
| TMAb/% | 1.009(0.972~1.050) | 0.480 | 0.632 | | | |
| TGAb/(IU/mL) | 1.000(0.999~1.001) | 0.561 | 0.575 | | | |
| TG/(ng/mL) | 0.999(0.993~1.005) | −0.212 | 0.832 | | | |
| TSH/(μIU/mL) | 1.013(0.876~1.183) | 0.176 | 0.861 | | | |
| FT4/(pmol/L) | 0.969(0.858~1.091) | −0.525 | 0.599 | | | |
| FT3/(pmol/L) | 0.963(0.678~1.011) | −0.418 | 0.676 | | | |
| T4/(nmol/L) | 0.996(0.982~1.010) | −0.577 | 0.564 | | | |
| T3/(nmol/L) | 0.951(0.424~2.137) | −0.123 | 0.902 | | | |

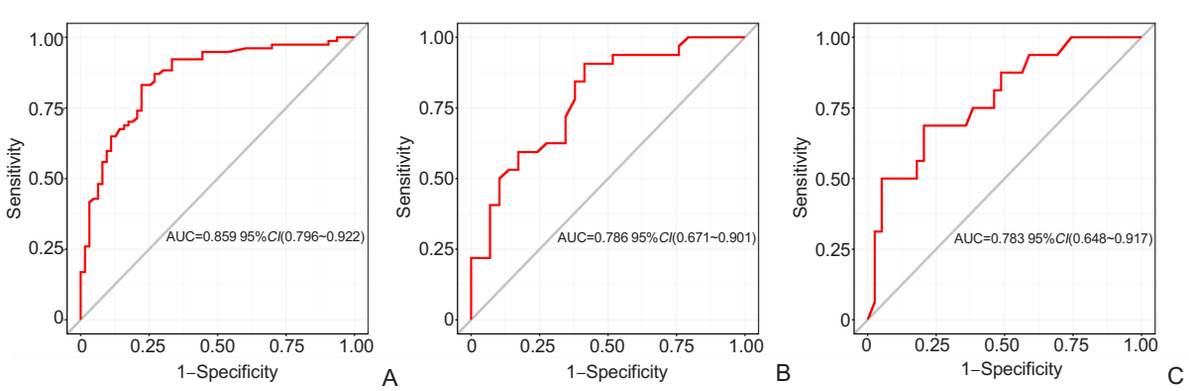



图3 训练集(A)、内部测试集(B)、外部测试集(C)中列线图预测模型的ROC曲线及AUC值

Figure 3 ROC curves and AUC values of the nomogram prediction model in the training set (A), internal test set (B), and external test set (C)

2.3 列线图模型的评价及验证

采用ROC判断模型的区分度,结果显示训练集列线图预测模型的曲线下面积(area under the curve, AUC)为0.859(95%*CI*:0.796~0.922);内部测试集中列线图预测模型的AUC为0.786(95%*CI*:0.671~0.901);外部测试集中列线图预测模型的AUC为0.783(95%*CI*:0.648~0.917);提示该预测模型具有良好的区分度(图3)。训练集、内部测试集及外部测试集的校准曲线显示模型的预测概率和实际概率接近,校准度良好(图4)。Hosmer-Lemeshow检验结果显示,

在训练集中X-squared=5.455 1, df=8, $P$=0.708;在内部测试集中X-squared=12.361, df=8, $P$=0.135 8,表明模型的拟合优度良好。

### 2.4 列线图预测模型的临床有效性分析

采用临床决策曲线对列线图预测模型进行临床适用性评价,结果显示,当训练集、内部测试集及外部测试集概率分别为0.18~1.00、0.18~0.80及0.10~0.55时,患者的净获益率大于0(图5)。

## 3 讨论

### 3.1 CLNM术前识别对PTMC个体化治疗的意义

颈部淋巴结转移是PTMC的常见模式,使得颈部淋巴结清扫至关重要。中央区颈淋巴结清扫显著影响患者的治疗、随访和预后[13]。关于颈部淋巴结转移的治疗,特别是关于预防性颈部淋巴结清扫,存在重大争议。鉴于PTMC患者经常发现中央区淋巴结受累,预防性中央区淋巴结清扫术(prophylactic central lymph node dissection,pCLND)被认为有助于降低复发和二次手术的风险,一些不同国家的多个指南积极强调了对PTMC患者的必要性[14-15]。中国临床肿瘤学会(Chinese Society of Clinical Oncology, CSCO)指南(2018版)建议,在全面评估PTMC患者的手术风险和益处后进行pCLND[16]。然而,一些研究人员反对预防性淋巴结清扫,因为其潜在并发症以及对患者生活质量的影响[17-18]。这场争论的中心问题是CLNM的准确术前识别。因此,术前可靠地确定PTMC中的CLNM对于制定有效的手术策略、优化肿瘤分期、预测局部复发和定制个体化治疗计划,最终提高患者预后至关重要。

### 3.2 CT影像特征协同临床指标提升CLNM风险分层效能

本研究中性别、肿瘤最大直径、被膜累及、CT诊断淋巴结是PTMC患者发生CLNM的独立风险因素。男性患者发生CLNM的风险显著高于女性患者,这与多项先前的研究结果一致[19-21]。此外,肿瘤最大直径作为一个关键的临床预测因子,较大的肿瘤尺寸与CLNM的发生密切相关,这进一步支持了肿瘤体积与淋巴结转移的相关性[20]。被膜累及也被认为是CLNM的独立风险因素,反映了肿瘤侵袭性与局部转移能力之间的密切关系[22]。CT诊断中发现的淋巴结异常也

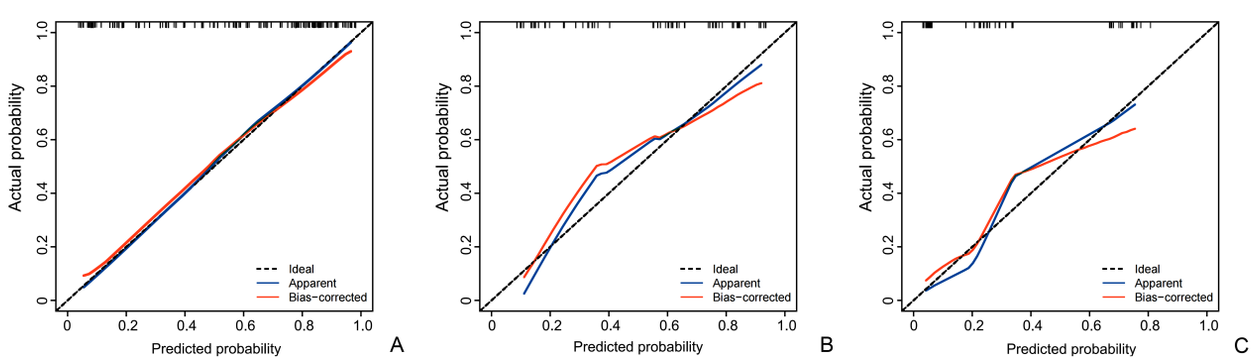



图4 训练集(A)、内部测试集(B)、外部测试集(C)中列线图预测模型的校准曲线

**Figure 4 Calibration curves of the nomogram prediction model in the training set (A), internal test set (B), and external test set (C)**

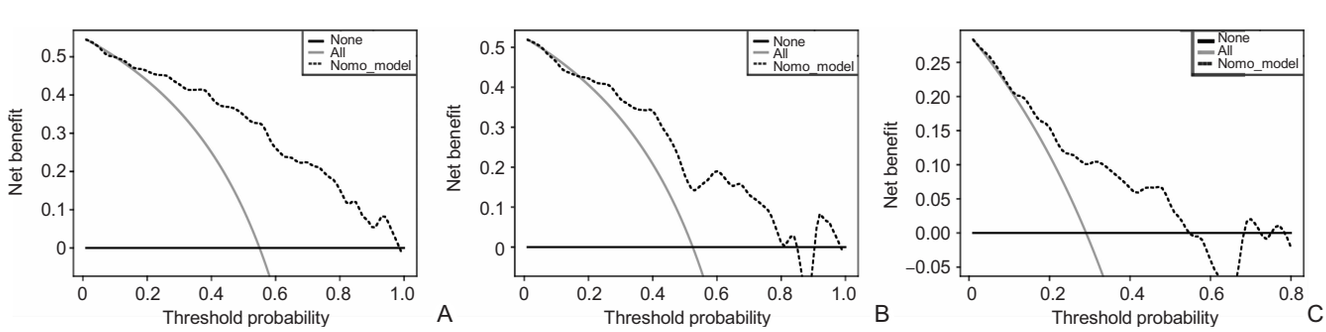



图5 在训练集(A)、内部测试集(B)、外部测试集(C)中列线图预测模型的临床决策曲线

**Figure 5 Clinical decision curves of the nomogram prediction model in the training set (A), internal test set (B), and external test set (C)**

提示可能存在CLNM,这与影像学检查在预测淋巴结转移中的重要性相符[23]。尽管如此,现有影像学方法仍面临若干挑战。例如,CT对小病灶的敏感性存在局限[24],尤其是在中央区淋巴结微小转移的检测上可能存在漏诊的风险。此外,CT图像的解读在不同临床中心可能存在一定差异,这在多中心大规模应用时可能影响诊断的准确性[25]。因此,尽管CT影像特征在分层CLNM风险方面具有一定优势,但其预测性能仍需结合其他影像学检查(如超声、MRI等)和分子标志物分析进行综合评估。

### 3.3 列线图模型提升CLNM术前识别精度与实用性

在本研究中,根据临床信息、术前CT检查最终建立了列线图模型,列线图模型实现了逻辑回归的可视化,该模型因有可视化、计算方便的优势而在近年得到了广泛的应用[26]。本研究根据术前CT影像特征及患者临床特征,较WANG等[27]依赖术后病理参数构建的模型更具临床实用性,较YE等[28]结合临床与超声特征的列线图(AUC=0.684)提升了预测精度。模型的临床校准曲线及决策曲线分析(decision curve analysis,DCA)结果表明,在阈值概率为0.18~0.80时,相较于无预测模型的传统方法,本模型能够显著提高CLNM的术前识别率,有助于满足患者个性化医疗的需求、优化资源配置和精确制定手术方案。

这项研究仍然有几个局限性:①由于本研究样本量比较小,因此,需要使用大样本数据进行后续评估。此外;②本研究的模型需要前瞻性的进一步验证,以确认其在现实世界环境中的诊断性能;③本研究的模型仅适用于PTMC,不适用于其他亚型的甲状腺癌;④由于一些患者的数据有限,基因组信息没有纳入本研究模型。现有文献表明,BRAFV600E突变的个体淋巴结转移风险可能增加[29-30]。因此,应该将定量成像特征与基因组表型相结合,并探索基于融合模型的生物学解释,以使本研究的模型更容易理解和更有价值,当拥有更大样本量的数据集时,本课题组将在未来的研究中验证目前的发现。本研究开发的基于CT特征与临床因素的列线图模型为PTMC患者中央区淋巴结转移的术前预测提供了一种新的方法。该模型在预测准确性和临床应用价值方面均显示出显著优势,未来的研究应继续优化该模型,并通过整合更多的生物学特征、外部验证数据和跨学科合作,进一步提高其在甲状腺癌个体化治疗中的临床效用。

**利益冲突** 本文所有作者声明不存在利益冲突

**参考文献:**

[1] MA T, WANG L L, ZHANG X Y, *et al*. A clinical and molecular pathology prediction model for central lymph node metastasis in CN0 papillary thyroid microcarcinoma[J]. Front Endocrinol, 2023, 14: 1075598. DOI: 10.3389/fendo.2023.1075598.

[2] BRITO J P, HAY I D. Management of papillary thyroid microcarcinoma[J]. Endocrinol Metab Clin North Am, 2019, 48(1): 199-213. DOI: 10.1016/j.ecl.2018.10.006.

[3] ITO Y, MIYAUCHI A. Active surveillance of low-risk papillary thyroid microcarcinomas[J]. Gland Surg, 2020, 9(5): 1663-1673. DOI: 10.21037/gs-2019-catp-03.

[4] ZHU Y Z, LIN J Y, YAN Y X, *et al*. Delphian lymph node metastasis is a novel indicator of tumor aggressiveness and poor prognosis in papillary thyroid cancer[J]. J Surg Oncol, 2021, 123(7): 1521-1528. DOI: 10.1002/jso.26380.

[5] MOON JH, LEE EK, CHA W, *et al*. Study protocol of expanded multicenter prospective cohort study of active surveillance on papillary thyroid microcarcinoma (MAESTRO-EXP). Endocrinol Metab. 2025; 40(2): 236-246. DOI:10.3803/EnM.2024.2136

[6] FRANCIS G L, WAGUESPACK S G, BAUER A J, *et al*. Management guidelines for children with thyroid nodules and differentiated thyroid cancer: the American Thyroid Association guidelines task force on pediatric thyroid cancer[J]. Thyroid, 2015, 25(7): 716-759. DOI: 10.1089/thy.2014.0460.

[7] WU L M, GU H Y, QU X H, *et al*. The accuracy of ultrasonography in the preoperative diagnosis of cervical lymph node metastasis in patients with papillary thyroid carcinoma: a meta-analysis[J]. Eur J Radiol, 2012, 81(8): 1798-1805. DOI: 10.1016/j.ejrad.2011.04.028.

[8] TONG Y Y, ZHANG J W, WEI Y, *et al*. Ultrasound-based radiomics analysis for preoperative prediction of central and lateral cervical lymph node metastasis in papillary thyroid carcinoma: a multi-institutional study [J]. BMC Med Imaging, 2022, 22(1): 82. DOI: 10.1186/s12880-022-00809-2.

[9] GAO L Y, WANG J J, JIANG Y X, *et al*. The number of central lymph nodes on preoperative ultrasound predicts central neck lymph node metastasis in papillary thyroid carcinoma: a prospective cohort study[J]. Int J Endocrinol, 2020, 2020: 2698659. DOI: 10.1155/2020/2698659.

[10] ALABOUSI M, ALABOUSI A, ADHAM S, *et al*. Diagnostic test accuracy of ultrasonography vs computed tomography for papillary thyroid cancer cervical lymph node metastasis: a systematic review and meta-analysis [J]. JAMA Otolaryngol Head Neck Surg, 2022, 148(2): 107-118. DOI: 10.1001/jamaoto.2021.3387.

[11] XING Z C, QIU Y X, YANG Q R, *et al*. Thyroid cancer neck lymph nodes metastasis: Meta-analysis of US and CT diagnosis [J]. Eur J Radiol, 2020, 129: 109103. DOI:

10.1016/j.ejrad.2020.109103.

[12] WU T, SUI G Q, TENG D K, *et al*. Study on changes in immune function after microwave ablation of papillary thyroid microcarcinoma[J]. Cancer Manag Res, 2022, 14: 2861-2868. DOI: 10.2147/CMAR.S358649.

[13] WANG Y J, WANG D Z, CHEN L L, *et al*. A comparison of two operation methods revealed the risk factors and the necessity of LN-prRLN dissection in papillary thyroid carcinoma: a retrospective cohort study in FUSCC[J]. Int J Endocrinol, 2020, 2020: 7162793. DOI: 10.1155/2020/7162793.

[14] ERASLAN G, AVSEC Ž, GAGNEUR J, *et al*. Deep learning: new computational modelling techniques for genomics[J]. Nat Rev Genet, 2019, 20(7): 389-403. DOI: 10.1038/s41576-019-0122-6.

[15] ZHOU L Q, WU X L, HUANG S Y, *et al*. Lymph node metastasis prediction from primary breast cancer US images using deep learning[J]. Radiology, 2020, 294(1): 19-28. DOI: 10.1148/radiol.2019190372.

[16] HOSNY A, PARMAR C, QUACKENBUSH J, *et al*. Artificial intelligence in radiology[J]. Nat Rev Cancer, 2018, 18(8): 500-510. DOI: 10.1038/s41568-018-0016-5.

[17] ROTSTEIN L. The role of lymphadenectomy in the management of papillary carcinoma of the thyroid[J]. J Surg Oncol, 2009, 99(4): 186-188. DOI: 10.1002/jso.21234.

[18] ZHONG X, LU Y P, YIN X, *et al*. Prophylactic central lymph node dissection performed selectively with CN0 papillary thyroid carcinoma according to a risk-scoring model[J]. Gland Surg, 2022, 11(2): 378-388. DOI: 10.21037/gs-21-906.

[19] QIU P J, GUO Q N, PAN K L, *et al*. Development of a nomogram for prediction of central lymph node metastasis of papillary thyroid microcarcinoma[J]. BMC Cancer, 2024, 24(1): 235. DOI: 10.1186/s12885-024-12004-3.

[20] WANG Z Y, GUI Z Q, WANG Z H, *et al*. Clinical and ultrasonic risk factors for high-volume central lymph node metastasis in CN0 papillary thyroid microcarcinoma: a retrospective study and meta-analysis[J]. Clin Endocrinol, 2023, 98(4): 609-621. DOI: 10.1111/cen.14834.

[21] OH H S, PARK S, KIM M, *et al*. Young age and male sex are predictors of large-volume central neck lymph node metastasis in clinical N0 papillary thyroid microcarcinomas[J]. Thyroid, 2017, 27(10): 1285-1290. DOI: 10.1089/thy.2017.0250.

[22] YU M, DENG J Q, GU Y H, *et al*. Preoperative high level of circulating tumor cells is an independent risk factor for central lymph node metastasis in papillary thyroid carcinoma with maximum lesion diameter ≤1.0 cm[J]. Int J Gen Med, 2024, 17: 4907-4916. DOI: 10.2147/IJGM.S487992.

[23] TIAN D D, LI X Q, JIA Z Z. Analysis of risk factors and risk prediction for cervical lymph node metastasis in thyroid papillary carcinoma[J]. Cancer Manag Res, 2024, 16: 1571-1585. DOI: 10.2147/CMAR.S485708.

[24] 崔晓剑, 潘婷, 郝锐, 等. PACS辅助系统与CT工作站诊断周围型肺癌准确性研究[J]. 空军军医大学学报, 2022, 43(7): 852-855. DOI: 10.13276/j.issn.2097-1656.2022.07.014.
CUI X J, PAN T, HAO R, *et al*. Accuracy study of PACS-assisted system and CT workstation in the diagnosis of peripheral lung cancer[J]. J Air Force Med Univ, 2022, 43(7): 852-855. DOI:10.13276/j.issn.2097-1656.2022.07.014.

[25] 李嘉宁, 张倩霞, 周子超, 等. 上颌第一磨牙解剖结构的锥形束CT研究[J]. 空军军医大学学报, 2024, 45(10): 1092-1098. DOI:10.13276/j.issn.2097-1656.2024.10.003.
LI J N, ZHANG Q X, ZHOU Z C, *et al*. A cone beam CT study of the anatomical structure of the maxillary first molar[J]. J Air Force Med Univ, 2024, 45(10): 1092-1098. DOI:10.13276/j.issn.2097-1656.2024.10.003.

[26] 成杰, 魏晓凡, 陈伟, 等. 基于增强CT术前诊断增殖型肝细胞癌的临床价值及预后分析[J]. 陆军军医大学学报, 2025, 47(7): 708-719. DOI: 10.16016/j.2097-0927.202411115.
CHENG J, WEI X F, CHEN W, *et al*. Clinical value and prognosis analysis of enhanced CT preoperative diagnosis for proliferative hepatocellular carcinoma[J]. J Army Med Univ, 2025, 47(7): 708-719. DOI: 10.16016/j.2097-0927.202411115.

[27] WANG D H, HU J, DENG C, *et al*. Predictive nomogram for central lymph node metastasis in papillary thyroid microcarcinoma based on pathological and ultrasound features[J]. Front Endocrinol, 2023, 14: 1108125. DOI: 10.3389/fendo.2023.1108125.

[28] YE J, FENG J W, WU W X, *et al*. Papillary thyroid microcarcinoma: a nomogram based on clinical and ultrasound features to improve the prediction of lymph node metastases in the central compartment[J]. Front Endocrinol, 2021, 12: 770824. DOI: 10.3389/fendo.2021.770824.

[29] CHEN T Y, LORCH J H, WONG K S, *et al*. Histological features of BRAF V600E-mutant anaplastic thyroid carcinoma[J]. Histopathology, 2020, 77(2): 314-320. DOI: 10.1111/his.14144.

[30] CELIK M, BULBUL B Y, AYTURK S, *et al*. The relation between BRAFV600E mutation and clinicopathological characteristics of papillary thyroid cancer[J]. Med Glasnik, 2019, 17(1): 30-34. DOI: 10.17392/1086-20.

(**收稿**:2025-06-09;**修回**:2025-08-25)

(编辑 李 玥)